

Cite this: *Catal. Sci. Technol.*, 2021, 11, 2456

Sewage-free preparation of 2D metal oxides by a rapid freezing soft template method for extraordinarily activating solar-driven humidity VOC combustion†

Dachao Yuan,^{‡a} Luping Ma,^a Jianguo Zhao,^a Xianhua Bai,^b Jianchang Li,^a Jianjun Hao^{*a} and Yaguang Li^{id *b}

Humidity volatile organic compounds (VOCs) cause significant harm to human beings. Two-dimensional (2D) metal oxides exhibit excellent activity towards humidity VOC catalytic combustion. Organic compounds as soft templates have been widely used in the preparation of 2D metal oxides. However, due to the structural fragility of soft templates, the mineralization process is necessary for acquiring 2D metal oxides, which results in the discharge of sewage. Herein, in this study, a novel soft template method based on rapid freezing to generally prepare 2D metal oxides without producing sewage is reported. It is worth emphasizing that the as-synthesized 2D Co_3O_4 has an 8 nm level of thickness and high specific surface area, which enable it to exhibit high activity towards the combustion VOCs, including formaldehyde, CH_4 , and acetone, and fully oxidize VOCs to CO_2 due to the excellent CO oxidation activity of 2D Co_3O_4 . Further, 2D Co_3O_4 is added into the light selective absorbing device to obtain a high temperature of 295 °C under 1 sun irradiation. Consequently, 2D Co_3O_4 shows a nearly 100% combustion efficiency towards humidity formaldehyde, CH_4 , acetone, and CO under ambient sunlight irradiation, comparable to the corresponding thermal catalytic reactions and far beyond the photocatalytic reactions, showing the potential for practical applications.

Received 4th January 2021,
Accepted 25th January 2021

DOI: 10.1039/d1cy00029b

rsc.li/catalysis

Introduction

Humidity volatile organic compounds (VOCs) are the main pollutant gases, which have adverse effects on human health.^{1,2} Due to the strong adsorption between water molecules and catalytic sites,³ VOCs are hardly adsorbed by the catalytic sites. It makes VOCs difficult to react and usually requires temperatures above 100 °C to avoid water condensation, causing energy consumption. Thermal catalytic combustion is the mainstream technology for the removal of VOCs with the merit of high catalytic efficiency.^{4,5} Metal oxides, such as Co_3O_4 ,⁶ CeO_2 ,^{7,8} MnO_x ,^{9,10} and LaMnO_3 ,¹¹ have exhibited excellent VOC removal efficiency. Among them, Co_3O_4 has high activity towards CO oxidation to CO_2 ,

ensuring the complete oxidation of VOCs into CO_2 (ref. 12) to avoid the secondary pollution of CO. Extensive efforts are used to exploit metal oxides for numerous types of catalytic reactions.^{13–15}

In particular, because of the bizarre electronic properties and large specific surface surfaces,^{16,17} the metal oxides synthesized in a two-dimensional (2D) nanosheet morphology are excellent candidates for numerous applications.^{18,19} To meet the mass production and low cost, organic compounds, such as P123 (ref. 20) and PVP,²¹ as soft templates have been widely used to synthesize 2D materials. Due to the structural fragility of soft templates, it is necessary to add a mineralizer to form 2D metal oxides.²⁰ Therefore, it requires a complex washing process to remove the mineralizer and obtain products, resulting in sewage discharge, which is harmful to the environment. In view of the green chemistry, overcoming the structural fragility of soft templates to omit sewage for synthesizing metal oxides as 2D nanosheets is highly desirable.

Herein, in order to solve the sewage discharge problem of the soft template method, we developed a novel soft template method to synthesize 2D metal oxides. In this method, a rapid freezing method was used to conquer the structural

^a College of Mechanical and Electrical Engineering, Hebei Agricultural University, Baoding 071001, P. R. China. E-mail: hjpaper@163.com

^b Hebei Key Lab of Optic-electronic Information and Materials, The College of Physics Science and Technology, Institute of Life Science and Green Development, Hebei University, Baoding, 071002, China. E-mail: liyaguang@hbu.edu.cn

† Electronic supplementary information (ESI) available. See DOI: 10.1039/d1cy00029b

‡ These authors contributed equally.

fragility of the soft templates to omit the mineralization process and washing process, thus resulting in zero sewage discharge during the synthesis of 2D metal oxides. Among the as-synthesized 2D materials, 2D Co_3O_4 has the merits of a porous structure and large specific surface area, which showed excellent activity towards the combustion of numerous humidity VOCs. Further, we developed a light selective absorbing device to nearly fully absorb sunlight and confine the sunlight converted heat energy to convert 1 sun irradiation to a 300 °C level high temperature.²² Consequently, the system of 2D Co_3O_4 supported by the light selective absorbing device exhibited high activity in ambient sunlight-driven humidity VOC combustion, which are comparable to corresponding thermal catalytic reactions and superior to the photocatalytic reactions.

Experimental section

Experimental details are given in the ESI.†

Results and discussion

Taking Co_3O_4 as an example, we showed the difference in the preparation principle between the traditional soft template method and rapid freezing soft template method. In this work, PVP was used as a soft template. $\text{Co}(\text{NO}_3)_2 \cdot 6\text{H}_2\text{O}$ and PVP were added to water to make a transparent aqueous solution. It is known that PVP is a typical soft template that can bond to Co ions as Co-PVP²¹ and form a two-dimensional micelle, as shown in Fig. 1a.²³ However, Co-PVP as a soft template is fragile, and the movement of the solution and solute molecules could lead to the collapse of the soft templates. Therefore, in the traditional soft template method,^{20,24} mineralizers (such as urea and Na_2CO_3) were added to form 2D hydroxides to obtain enough rigidity (Fig. 1b), and the impurities are formed as well. The subsequent washing process was used to remove impurities, thus inevitably producing wastewater, as shown in Fig. 1c. In our method, we used liquid nitrogen to quickly freeze the

solution containing Co-PVP into ice (Fig. 1d). Then, the water was removed by freeze-drying to obtain Co-PVP. Fig. S1† shows that the morphology of Co-PVP is a uniform two-dimensional morphology, and as depicted in Fig. 1e, we could use the rapid freezing method to retain the 2D morphology of Co-PVP without adding any mineralizer. Therefore, the washing process and wastewater were absent from the whole synthesis process. After the subsequent annealing treatment, we could obtain Co_3O_4 in 2D morphology, named as 2D Co_3O_4 (Fig. 1f).

From the XRD pattern in Fig. S2a,† we can see that cubic phase Co_3O_4 (JCPDS no. 43-1003) existed in 2D Co_3O_4 . The peaks at 19°, 31.3°, 36.9°, 38.2°, 44.5°, 55.6°, 59.4°, and 65.3° are assigned to the (111), (220), (311), (222), (400), (422), (511), and (440) planes, respectively.²⁵ SEM and TEM techniques were employed to visualize the morphology and structure of 2D Co_3O_4 . It was clear that 2D Co_3O_4 exhibited a 2D structure (Fig. 2a). The 2D morphology of 2D Co_3O_4 was further confirmed by enlarged SEM and TEM images (Fig. 2b and c), and they revealed that 2D Co_3O_4 has a porous morphology, which might be caused by the decomposition of PVP. The high-resolution TEM (HRTEM) image in Fig. 2d showed that 2D Co_3O_4 exhibited clear lattice fringes from the (220) plane of cubic Co_3O_4 with a lattice spacing of 0.286 nm. The thickness of 2D Co_3O_4 was 8.8 nm (Fig. S2b†). From the EDS mapping of 2D Co_3O_4 , we could see that oxygen and cobalt were uniformly dispersed (Fig. S2c and d†). Based on this strategy, we successfully obtained other 2D metal oxides, including CuO (Fig. S3a and d†), ZnO (Fig. S3b and e†), and Fe_2O_3 (Fig. S3c and f†), representing the universality of this method for synthesizing 2D metal oxides.

The nitrogen isotherms of 2D Co_3O_4 show typical IV type with hysteresis loops, indicating that the mesoporous

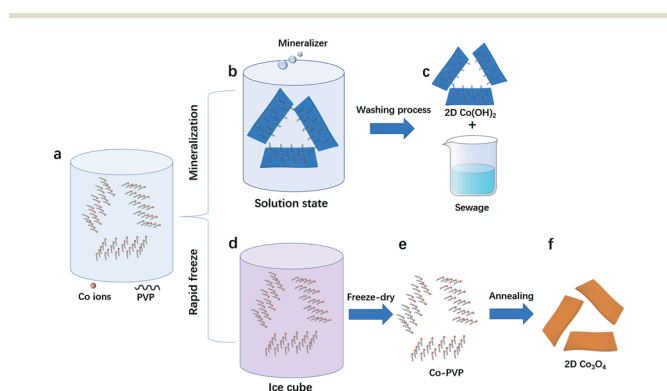


Fig. 1 Preparation diagram of 2D Co_3O_4 via the traditional soft template method (a–c) and rapid freezing soft template method (a and d–f) at different stages.

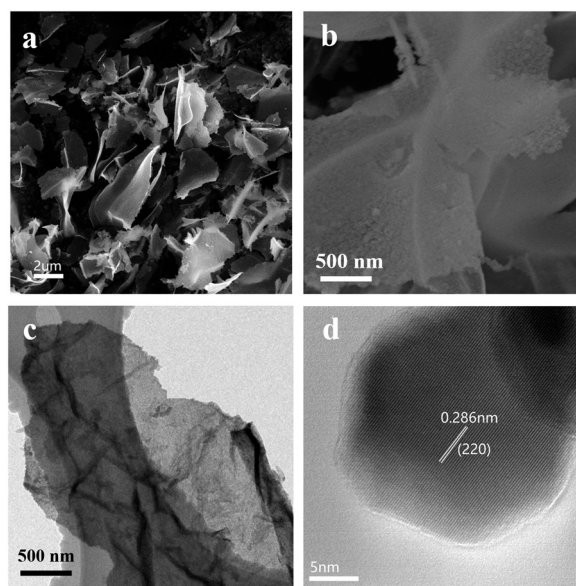


Fig. 2 (a and b) SEM images, (c) TEM image, (d) HRTEM image of 2D Co_3O_4 .

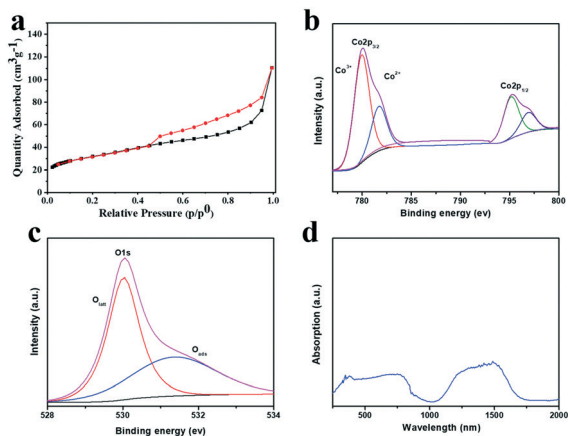


Fig. 3 (a) N_2 adsorption-desorption isotherm of 2D Co_3O_4 . (b and c) XPS spectra of Co and O elements from 2D Co_3O_4 . (d) UV-vis-IR absorption spectra of 2D Co_3O_4 .

structure is present in 2D Co_3O_4 (Fig. 3a). This can be further proved by the pore size distribution (Fig. S4[†]). The specific surface area of 2D Co_3O_4 was calculated to be $115.9 \text{ m}^2 \text{ g}^{-1}$. The high surface area and porous structure of 2D Co_3O_4 would be beneficial for the catalytic reactions in terms of the mass transfer and accessibility of active catalysts to the reactant. As displayed in Fig. 3b, the spectrum of Co 2p from 2D Co_3O_4 showed spin-orbit splitting into $2p_{1/2}$ and $2p_{3/2}$ components. Both components contain the same qualitative information, and Co $2p_{3/2}$ had two components at the band energy (BE) values of 777.95 and 781.75 eV, and Co $2p_{1/2}$ also had two components with BE of 795.35 and 796.35 eV, which were assigned to Co^{3+} and Co^{2+} ions, respectively.²⁶ Fig. 3c shows that O1s had signals displayed at the BE values of 529.9 and 531.3 eV. The former was surface lattice oxygen (O_{latt}),^{27,28} whereas the latter was surface adsorption oxygen (O_{ads}).^{26,29} The presence of surface-active oxygen species and Co^{3+} cationic species were beneficial to promote the catalytic process. The UV-vis-IR spectrum (Fig. 3d) shows a typical light absorption spectrum of 2D Co_3O_4 with full light absorption throughout the whole solar spectrum.

2D Co_3O_4 showed high activity towards numerous types of humidity VOC catalytic reactions. Fig. 4 shows the catalytic performance of 2D Co_3O_4 , compared with that of nano Co_3O_4 synthesized by the sol-gel method (Fig. S5[†]), which had a porous morphology and specific surface area of $33.2 \text{ m}^2 \text{ g}^{-1}$ (Fig. S5c[†]). The feed gas was a mixture of O_2/N_2 with a volume ratio of 20%/80% passed through water, and the concentration of humidity VOCs (formaldehyde, CH_4 , and acetone) was 1000 ppm. As shown in Fig. 4a, nano Co_3O_4 shows poor catalytic activity towards the complete conversion of 1000 ppm of formaldehyde at a high temperature of 180 °C, while 2D Co_3O_4 can entirely oxidize 1000 ppm of formaldehyde at a low temperature of 120 °C. Not only formaldehyde, but 2D Co_3O_4 could also catalytically oxidize 97% of CH_4 and 98% of acetone at 300 °C, in comparison with 18% of CH_4 and 55% of acetone using nano Co_3O_4 at corresponding temperatures (Fig. 4b and c). The superior

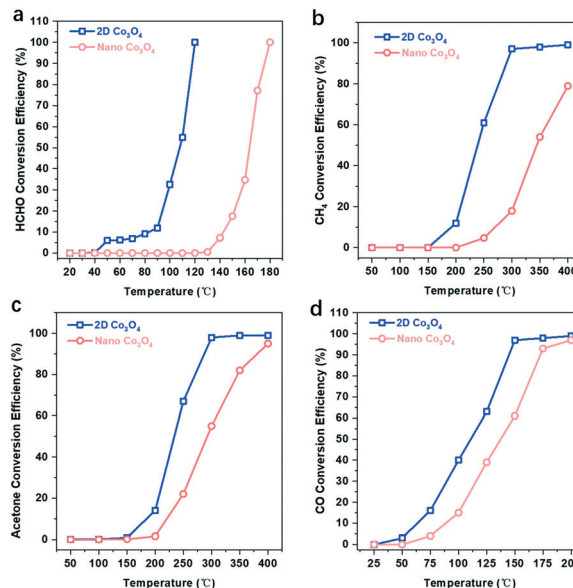


Fig. 4 Temperature-dependent formaldehyde oxidation (a), CH_4 oxidation (b), acetone oxidation (c), and CO oxidation (d) of 2D Co_3O_4 and nano Co_3O_4 .

VOC oxidation performance of 2D Co_3O_4 should be ascribed to the porous structure and large surface area. Fig. S6–S8[†] shows that nearly 100% selectivity towards CO_2 formation was achieved in the oxidation of formaldehyde, CH_4 , and acetone at 120 °C, 300 °C, 300 °C through 2D Co_3O_4 . Fig. 4d shows that 2D Co_3O_4 and nano Co_3O_4 could catalytically oxidize 97% and 61% of CO to CO_2 at 150 °C, respectively. The excellent CO oxidation activity should be the main reason for the full oxidation of VOCs of 2D Co_3O_4 . Fig. S9[†] shows the catalytic stability characterization of formaldehyde, CH_4 , CO, and acetone at the temperature of 120 °C, 300 °C, 150 °C, 300 °C, respectively, and it showed that 2D Co_3O_4 exhibited excellent stability towards all the VOC tests.

With efficient catalysts, we plan to use sunlight to replace traditional energy on driving the catalytic reactions. At present, the main catalysis driven by sunlight is photocatalysis, *i.e.*, sunlight-photogenerated electron and hole-chemicals. In addition to photocatalysis, the sunlight-driven thermal catalysis is another strategy,^{4,24,30,31} that is, sunlight thermal energy chemicals. As shown in Fig. 5a, different from the direct irradiation of sunlight in photothermal catalysis, we constructed a reaction tube as a light selective absorbing device by decorating it with a spectrally selective coating and vacuum layer. 2D Co_3O_4 was loaded in the interior of the reaction tube. In this system, the spectrally selective coating was used to absorb sunlight and generate thermal energy. The light absorbance of the spectrally selective coating was completely different from that of 2D Co_3O_4 . The spectrum absorption curve of spectrally selective coating and 2D Co_3O_4 indicated a high light absorption ranging from 0.4–2.0 μm (Fig. 5b), revealing the nearly full sunlight absorption property. In addition, spectrally selective coating and 2D Co_3O_4 showed nearly zero

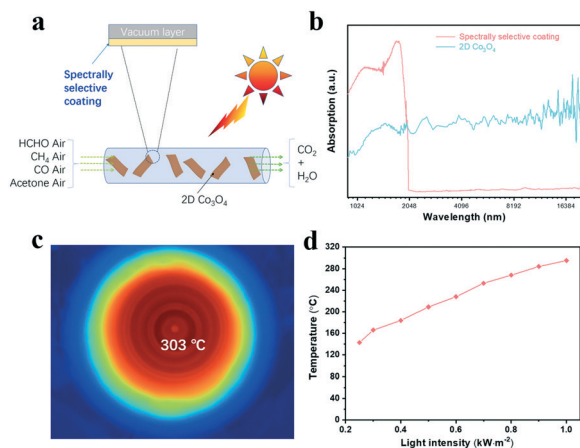


Fig. 5 (a) Sketch map of the reaction tube with the spectrally selective coating and vacuum layer. (b) Normalized light absorption spectra of the spectrally selective coating and 2D Co_3O_4 ranging from 0.4 to 20 μm . (c) The IR mapping of the spectrally selective coating under 1 sun irradiation. (d) The temperature of 2D Co_3O_4 loaded in the spectrally selective coating-based reaction tube under sunlight irradiation with different intensities.

light absorption and violent light absorption, respectively, and also at the infrared (IR) region of 3–20 μm (Fig. 5b). Kirchhoff's law has evidenced that the materials having high IR absorption could emit more heat energy by IR radiation.³² We used an IR camera to detect the temperature of the spectrally selective coating and 2D Co_3O_4 under 1 sun irradiation (1 kW m^{-2}). The infrared (IR) images show that the temperature of the spectrally selective coating and 2D Co_3O_4 was 303 °C (Fig. 5c) and 75.4 °C (Fig. S10†), respectively, under 1 sun irradiation. It confirmed that the spectrally selective coating could create ultrahigh temperature just under ambient sunlight irradiation due to its property of high sunlight absorption and low IR radiation. As 2D Co_3O_4 was loaded in the light selective absorbing device, the high temperature could be used to heat 2D Co_3O_4 , which reached 140 and 295 °C under 0.25 and 1 sun irradiation, respectively (Fig. 5d), and capable of operating under numerous types of catalytic reactions.

We have carried out the photocatalysis of 2D Co_3O_4 (named as 2D Co_3O_4) and sunlight-driven thermal catalysis of 2D Co_3O_4 loaded in a light selective absorbing device, as shown in Fig. 5a (named as 2D Co_3O_4 + device). Fig. 6a–d show that 2D Co_3O_4 + device could eliminate almost 100% formaldehyde, CH_4 , acetone, and CO when the irradiated sunlight was higher than 0.25 sun, 1 sun, 1 sun, and 0.3 sun, respectively, comparable to the thermal catalytic humidity VOC combustion, as shown in Fig. 4. However, 2D Co_3O_4 only showed 10%, 0%, 0%, and 0% of the elimination rate for formaldehyde, CH_4 , acetone, and CO, respectively, under 1 sun irradiation. Compared with other sunlight-driven VOC elimination systems, under 1 sun irradiation, the photocatalytic removal efficiency for CH_4 , acetone, and CO was very low, almost only 1/100 of the efficiency of 2D Co_3O_4 + device,^{33–35} and photocatalytic removal of formaldehyde

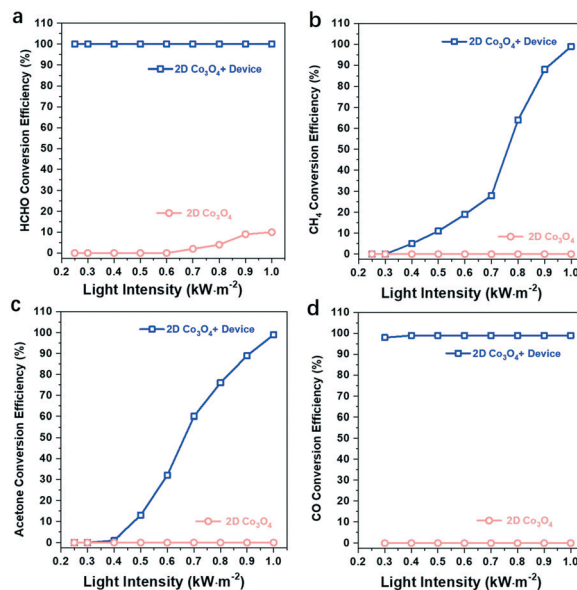


Fig. 6 The efficiency of formaldehyde oxidation (a), CH_4 oxidation (b), acetone oxidation (c), and CO oxidation (d) for 2D Co_3O_4 + device and 2D Co_3O_4 under sunlight irradiation with different intensities.

showed a relatively higher efficiency. Table S1† lists the state-of-the-art photocatalytic formaldehyde removal performances. To the best of our knowledge, the best reported turnover frequency (TOF) value was 0.138 min^{-1} under 1 sun irradiation.³⁶ We increased the inlet air rate to 500 sccm to test the maximum formaldehyde oxidation rate of the 2D Co_3O_4 + device under 1 sun irradiation, and the formaldehyde oxidation performance is depicted in Fig. S11†. Fig. S11† shows that the maximum formaldehyde oxidation concentration was about 47 293 ppm when the light intensity increased to 1 sun. We assumed that all Co atoms in 2D Co_3O_4 were used in this reaction, and TOF of formaldehyde oxidation through this system was 5.1 min^{-1} under 1 sun irradiation without additional energy import. It confirmed that the conversion rate of formaldehyde through the light selective absorbing device-assisted 2D Co_3O_4 was 37 times of the best reported photocatalytic formaldehyde decomposition value. The formaldehyde catalytic oxidation stability of the 2D Co_3O_4 + device was also recorded. As shown in Fig. S12†, the formaldehyde oxidation concentration over the light selective absorbing device-supported 2D Co_3O_4 remained the same after a 10 h test, indicating the highly stable sunlight-driven formaldehyde oxidation under 1 sun irradiation.

Conclusion

In this study, we have developed a rapid freezing soft template method to prepare 2D metal oxides, including Co_3O_4 , CuO, ZnO, and Fe_2O_3 , without producing wastewater. The obtained 2D Co_3O_4 catalyst possessed a porous structure and a large specific surface area of $115.9 \text{ m}^2 \text{ g}^{-1}$. As a result, the 2D Co_3O_4 catalyst showed the complete oxidation of humidity formaldehyde, CH_4 , acetone, and CO at 120 °C, 300

°C, 300 °C, and 150 °C, respectively. Furthermore, a novel photothermal conversion device was constructed using the spectrally selective coating, Cu film, and vacuum layer, which can heat 2D Co₃O₄ to 140 and 295 °C under 0.25 and 1 sun irradiation, respectively. Thus, 2D Co₃O₄ loaded in the light selective absorbing device could eliminate nearly 100% humidity formaldehyde, CH₄, acetone, and CO when the irradiated sunlight was higher than 0.25 sun, 1 sun, 1 sun, and 0.4 sun, respectively. The TOF of formaldehyde oxidation through this system was 5.1 min⁻¹ under 1 sun irradiation, 37 times higher than that of the state of the art photocatalytic formaldehyde decomposition.

Conflicts of interest

There are no conflicts to declare.

Acknowledgements

This work is supported by the National Nature Science Foundation of China (Grant No. 51702078), Hebei Provincial Department of Education Foundation (Grant No. BJ2019016), and the Advanced Talents Incubation Program of the Hebei University (521000981248). Thanks for the TEM technical supports provided by the Microanalysis Center, College of Physics Science and Technology, Hebei University.

References

- 1 T. Salthammer, S. Mentese and R. Marutzky, *Chem. Rev.*, 2010, **110**, 2536–2572.
- 2 A. Khan, R. Zheng, Y. Kan, J. Ye, J. Xing and Y. J. Zhang, *Angew. Chem., Int. Ed.*, 2014, **53**, 6439–6442.
- 3 Z. Bian, Y. Feng, H. Li and J. Zhan, *Environ. Res.*, 2020, **190**, 109984.
- 4 B. Li, D. Yuan, L. Ma, C. Shi and Y. Li, *Sci. Total Environ.*, 2020, **749**, 141595.
- 5 I. C. Dedoussi, S. D. Eastham, E. Monier and S. R. H. Barrett, *Nature*, 2020, **578**, 261–265.
- 6 Y. Wang, A. Zhu, B. Chen, M. Crocker and C. Shi, *Catal. Commun.*, 2013, **36**, 52–57.
- 7 Y. Huang, H. Li, M.-S. Balogun, H. Yang, Y. Tong, X. Lu and H. Ji, *RSC Adv.*, 2015, **5**, 7729–7733.
- 8 Q. Jin, A. Wang, B. Lu, X. Xu, Y. Shen and Y. Zeng, *Catal. Sci. Technol.*, 2020, **10**, 4436–4447.
- 9 J. Zhang, Y. Li, L. Wang, C. Zhang and H. He, *Catal. Sci. Technol.*, 2015, **5**, 2305–2313.
- 10 S. Rong, K. Li, P. Zhang, F. Liu and J. Zhang, *Catal. Sci. Technol.*, 2018, **8**, 1799–1812.
- 11 R. Spinicci, M. Faticanti, P. Marini, S. De Rossi and P. Porta, *J. Mol. Catal. A: Chem.*, 2003, **197**, 147–155.
- 12 X. Xie, Y. Li, Z.-Q. Liu, M. Haruta and W. Shen, *Nature*, 2009, **458**, 746–749.
- 13 R. R. Rao, M. J. Kolb, L. Giordano, A. F. Pedersen, Y. Katayama, J. Hwang, A. Mehta, H. You, J. R. Lunger, H. Zhou, N. B. Halck, T. Vegge, I. Chorkendorff, I. E. L. Stephens and Y. Shao-Horn, *Nat. Catal.*, 2020, **3**, 516–525.
- 14 D. W. Wakerley, M. F. Kuehnel, K. L. Orchard, K. H. Ly, T. E. Rosser and E. Reisner, *Nat. Energy*, 2017, **2**, 17021.
- 15 Y. A. Wu, I. McNulty, C. Liu, K. C. Lau, Q. Liu, A. P. Paulikas, C.-J. Sun, Z. Cai, J. R. Guest, Y. Ren, V. Stamenkovic, L. A. Curtiss, Y. Liu and T. Rajh, *Nat. Energy*, 2019, **4**, 957–968.
- 16 C. Zhang, A. Wang, J. Zhang, X. Guan, W. Tang and J. Luo, *Adv. Energy Mater.*, 2018, **8**, 1802833.
- 17 C. J. Heard, J. Čejka, M. Opanasenko, P. Nachtigall, G. Centi and S. Perathoner, *Adv. Mater.*, 2019, **31**, 1801712.
- 18 H. Liu, K. Tian, J. Ning, Y. Zhong, Z. Zhang and Y. Hu, *ACS Catal.*, 2019, **9**, 1211–1219.
- 19 H. Liu, L. Li, C. Guo, J. Ning, Y. Zhong and Y. Hu, *Chem. Eng. J.*, 2020, **385**, 123929.
- 20 Z. Sun, T. Liao, Y. Dou, S. M. Hwang, M.-S. Park, L. Jiang, J. H. Kim and S. X. Dou, *Nat. Commun.*, 2014, **5**, 3813.
- 21 H. Duan, N. Yan, R. Yu, C.-R. Chang, G. Zhou, H.-S. Hu, H. Rong, Z. Niu, J. Mao, H. Asakura, T. Tanaka, P. J. Dyson, J. Li and Y. Li, *Nat. Commun.*, 2014, **5**, 3093.
- 22 C. Shi, D. Yuan, L. Ma, G. Fu, S. Wang and Y. Li, *J. Cleaner Prod.*, 2020, 125328.
- 23 Y. H. Lee, C. L. Lay, W. Shi, H. K. Lee, Y. Yang, S. Li and X. Y. Ling, *Nat. Commun.*, 2018, **9**, 2769.
- 24 C. Shi, D. Yuan, L. Ma, Y. Li, Y. Lu, L. Gao, X. San, S. Wang and G. Fu, *J. Mater. Chem. A*, 2020, **8**, 19467–19472.
- 25 M. Casas-Cabanas, G. Binotto, D. Larcher, A. Lecup, V. Giordani and J. M. Tarascon, *Chem. Mater.*, 2009, **21**, 1939–1947.
- 26 J. Chen, Y. Zhang, L. Tan and Y. Zhang, *Ind. Eng. Chem. Res.*, 2011, **50**, 4212–4215.
- 27 L. Li, C. Guo, J. Shen, J. Ning, Y. Zhong and Y. Hu, *Chem. Eng. J.*, 2020, **400**, 125925.
- 28 B. He, H. Liu, Z. Lin, L. Yan, J. Ning, Y. Zhong, C. Zheng, Z. Zhang and Y. Hu, *Chem. Eng. J.*, 2019, **359**, 924–932.
- 29 Y. Xia, H. Dai, H. Jiang and L. Zhang, *Catal. Commun.*, 2010, **11**, 1171–1175.
- 30 Y. Li, J. Hao, H. Song, F. Zhang, X. Bai, X. Meng, H. Zhang, S. Wang, Y. Hu and J. Ye, *Nat. Commun.*, 2019, **10**, 2359.
- 31 X. Bai, D. Yuan, Y. Xu, Y. Li, W. Lu, S. Wang, G. Fu and Y. Hu, *Sol. Energy Mater. Sol. Cells*, 2020, **208**, 110395.
- 32 Z. Lou, D. Yuan, F. Zhang, Y. Wang, Y. Li and L. Zhu, *Nano Energy*, 2019, **62**, 653–659.
- 33 C. L. Bianchi, S. Gatto, C. Pirola, A. Naldoni, A. Di Michele, G. Cerrato, V. Crocellà and V. Capucci, *Appl. Catal., B*, 2014, **146**, 123–130.
- 34 M. Kask, J. Bolobajev and M. Krichevskaya, *Chem. Eng. J.*, 2020, **399**, 125815.
- 35 X. Qian, D. Yue, Z. Tian, M. Reng, Y. Zhu, M. Kan, T. Zhang and Y. Zhao, *Appl. Catal., B*, 2016, **193**, 16–21.
- 36 Z. Wan and G. Zhang, *J. Mater. Chem. A*, 2015, **3**, 16737–16745.